# Mechanistic Modeling of Polymer Degradation: A Comprehensive Study of Polystyrene

**Todd M. Kruse, Oh Sang Woo, Hsi-Wu Wong, Shumaila S. Khan, and Linda J. Broadbelt***

*Department of Chemical Engineering, Northwestern University, Evanston, Illinois 60208*

*Received March 28, 2002; Revised Manuscript Received July 15, 2002*

ABSTRACT: The degradation of polystyrene was modeled at the mechanistic level by developing differential equations describing the evolution of the moments of structurally distinct polymer species. This work extends our previous modeling work[1] by incorporating chain-length-dependent rate parameters, tracking branched species more explicitly, using rate parameters primarily from the literature, and comparing the model results to extensive experimental data on the degradation of polymers of different molecular weights and at different temperatures. Unique polymer groups were devised that allowed the necessary polymeric features for capturing the degradation chemistry to be tracked, while maintaining a manageable model size. The conversion among the species was described using typical free radical reaction types, including hydrogen abstraction, midchain $\beta$-scission, end-chain $\beta$-scission, 1,5-hydrogen transfer, 1,3-hydrogen transfer, radical addition, bond fission, radical recombination, and disproportionation. The model included over 2700 reactions and tracked 64 species. Programs were developed using the programming language Perl to assemble moment equations from input of the polymeric features to be tracked. The intrinsic kinetic parameters (a frequency factor and activation energy for each reaction) were obtained from data in the literature and previous modeling work in our laboratory.[2−4] The model predictions for the evolution of $M_n$ and $M_w$ and the yields of styrene, dimer, and trimer compare very well with experimental data obtained in our laboratory for the degradation of polystyrene over a large temperature range and with different initial molecular weights. Evolution of low molecular weight products from experiments reported in the literature is also captured.

## Introduction

Pyrolysis of polymeric materials has grown as a resource recovery strategy in recent years[5−9] and has a high potential for growth in the coming years provided that economically feasible processes can be developed.[10] Value is recovered from spent materials by converting polymers into fuels and chemicals and recovering monomer to produce new polymer.[11] However, a very diverse product distribution is typically formed during polymer pyrolysis due to the high temperatures used and the complex free radical reactions involved. An understanding of the interplay between the process conditions and the products obtained is needed to predict the full molecular weight range of products.

One valuable tool that can be used to capture the mechanistic chemistry directing the decomposition of polymeric materials via pyrolysis is kinetic modeling. One of the obstacles to constructing a kinetic model for polymeric systems is maintaining a manageable model size. As polydisperse, high molecular weight materials are pyrolyzed, polymeric chains of thousands of different lengths with different chemical compositions (i.e., numbers of branches, presence and position of a radical center, and location of double bonds) are formed. Tracking each one of these distinct species individually is too computationally demanding for the current hardware available. To overcome these difficulties, population-balance-based models have been developed using the method of moments to model molecular weight changes and small molecule evolution simultaneously.[12−21]

The framework for developing moment equations for polymer degradation using the theory of reactions in continuous mixtures has been developed in a series of papers by McCoy and co-workers.[12−21] In their procedure, the method of moments is applied to rate equations written explicitly in terms of chain length to develop differential equations describing the evolution of the moments. The moment equations are then solved to monitor the molecular weight distribution as a function of time. The majority of the models developed using this approach use global rate coefficients to quantify the kinetics. However, these models have been modified to describe the evolution of specific, low molecular weight products. Studies by Teymour and Campbell[22] and more recent work by Kodera and McCoy[23] and Pladis and Kiparissides[24] are examples in which moment equations were developed based on mechanistic chemistry by describing the moments of both "dead" and "live" polymer chains. As a whole, these works outline procedures for developing moment equations for a variety of free radical reaction types.

In previous work,[1] we combined these approaches to modeling polymer degradation and polymerization to develop a detailed mechanistic model for polymer degradation, and we extended these approaches in the following ways: (1) distinguished among different types of dead and live species according to the number of branches, the number of double bonds, the "head" or

* To whom correspondence should be addressed. Fax 847-491-3728. E-mail: broadbelt@northwestern.edu.

10.1021/ma020490a CCC: $22.00 
Published on Web 08/29/2002

"tail" orientation of the end units, and the position of the radical center to maintain a more direct link between structure and reactivity; (2) included additional reaction types; (3) specified rate constants for individual mechanistic steps in the context of a particular experimental system; (4) removed the assumption of the pseudo steady state approximation; and (5) compared the model results to experimental data. However, we have since advanced our original development by incorporating chain-length-dependent rate parameters, tracking branched species more explicitly, using rate parameters primarily from the literature, and comparing the model results to extensive experimental data on the degradation of polymers of different molecular weights and at different temperatures. One challenge to implementing this level of detail is the amount of information and bookkeeping required. A balance must be struck between a fully speciated model and one that does not possess sufficient detail to either capture the experimental measures of interest or differentiate the reactivities of chains with different structural features.

To overcome these obstacles, our work concentrated on developing the necessary framework for mechanistic modeling of the decomposition of polymers during pyrolysis by focusing first on the degradation of polystyrene, a voluminous component of mixed plastic waste. Detailed information about the decomposition of polystyrene was obtained from experiments in our laboratory.[2,25] The number-average molecular weight ($M_n$), the weight-average molecular weight ($M_w$), and the yield of specific low molecular weight products as a function of time were measured for polystyrene degradation in a batch reactor. The degradation of polystyrene with different initial molecular weights ($M_n$ = 5160, 42 500, 50 550, and 98 100) and at different temperatures (310, 350, 380, and 420 °C) was performed.

Differential equations tracking the moments of structurally distinct polymer species were developed, and these equations incorporated a wide range of free radical reactions, including reactions leading to specific low molecular weight products. Bond fission, chain-end $\beta$-scission, midchain $\beta$-scission, 1,5-hydrogen transfer, 1,3-hydrogen transfer, radical addition, radical recombination, disproportionation, and hydrogen abstraction were included. Unique polymer groups were devised that allowed polymeric features to be tracked while maintaining a manageable model size. Polymer species were lumped into various classes, as done previously,[1,24,26] to track the presence and location of radical centers, the position of double bonds, the inclusion of branches, and the orientation of the "head" and "tail" ends of the monomer units. The model developed tracked all major low molecular weight products, consisted of over 2700 reactions, and tracked 64 species.

To facilitate model construction, programs were developed using the programming language Perl to assemble moment equations from input of the polymeric features to be tracked. The intrinsic kinetic parameters (a frequency factor and activation energy for each reaction) were obtained from data in the literature and previous modeling work in our laboratory.[2−4] The approach to model construction, the detailed chemistry included, the quantitative parameters used, and comparison to experimental data are discussed below.

## Model Development

**Mechanistic Chemistry.** To track the evolution of the molecular weight distribution and the yields of lowmolecular weight products during pyrolysis, the method of moments was used to develop differential equations describing the pyrolysis kinetics. To implement the mechanistic chemistry of interest, the terms of the moment equations corresponding to each reaction type were derived from mass action kinetics of elementary steps and the method of moments. The terms of the moment equations were derived for the following reactions: (1) chain fission, (2) radical recombination, (3) allyl chain fission, (4) hydrogen abstraction, (5) midchain $\beta$-scission, (6) radical addition, (7) end-chain $\beta$-scission, (8) 1,5-hydrogen transfer (also 1,3-transfer), and (9) disproportionation. Examples of these reactions for polystyrene are pictured in Figure 1. The 1,3- and 1,5-hydrogen transfer reactions are well-known to occur in polystyrene degradation.[27] The subsequent $\beta$-scission of the specific radical formed by the 1,3-radical rearrangement produces dimer (2,4-diphenyl-1-butene) or a benzyl radical, and the subsequent $\beta$-scission of the specific radical formed by the 1,5- radical rearrangement produces trimer (2,4,6-triphenyl-1-hexene) or a 1,3-diphenyl-1-propyl radical.

The literature provided guidance for the derivations of the moment equations. However, either a less extensive set of reaction types or fewer distinct species were considered or chemistry at the pathways level, i.e., without considering radical intermediates, was implemented. The general form of moment equations including generation and consumption terms representing free radical polymerization reaction types is presented elsewhere,[12,18,22−24] but these expressions had to be manipulated to link structure directly to reactivity. In addition, the approach outlined by McCoy and Wang for describing random and proportioned chain fission and $\beta$-scission reactions[12,18] was utilized in the moment equations. Chain fission and midchain $\beta$-scission of linear chains were assumed to occur at random points along polymer chains, while the fission and scission of branched species were assumed to have both proportional and random characteristics.

**Moment Equations for Chain Fission/Radical Recombination.** Chain fission and radical recombination can be represented as shown in reaction a in terms of dead polymer (D) and end-chain radicals (Re) where the subscripts denote the chain lengths in terms of the number of monomer units. Moment equations for this reaction have been developed by McCoy and co-workers,[12,18] and these equations have been extended here to obtain eq 2 for the dead polymer which takes into account that there are two bonds per monomer unit that can undergo fission within a polymer chain (the superscripts denote the moments). The $e_f$ variable represents the number of bonds along a polymer chain that are excluded from this general chain fission reaction (such as unsaturated bonds that have a high bond strength). Equation 3 is the Saidel−Katz approximation for the third moment,[28] which is needed to obtain a closure on the differential equations for the moments of dead polymeric species. Moment equations have also been developed for the end-chain radicals[12,18,22] and are given

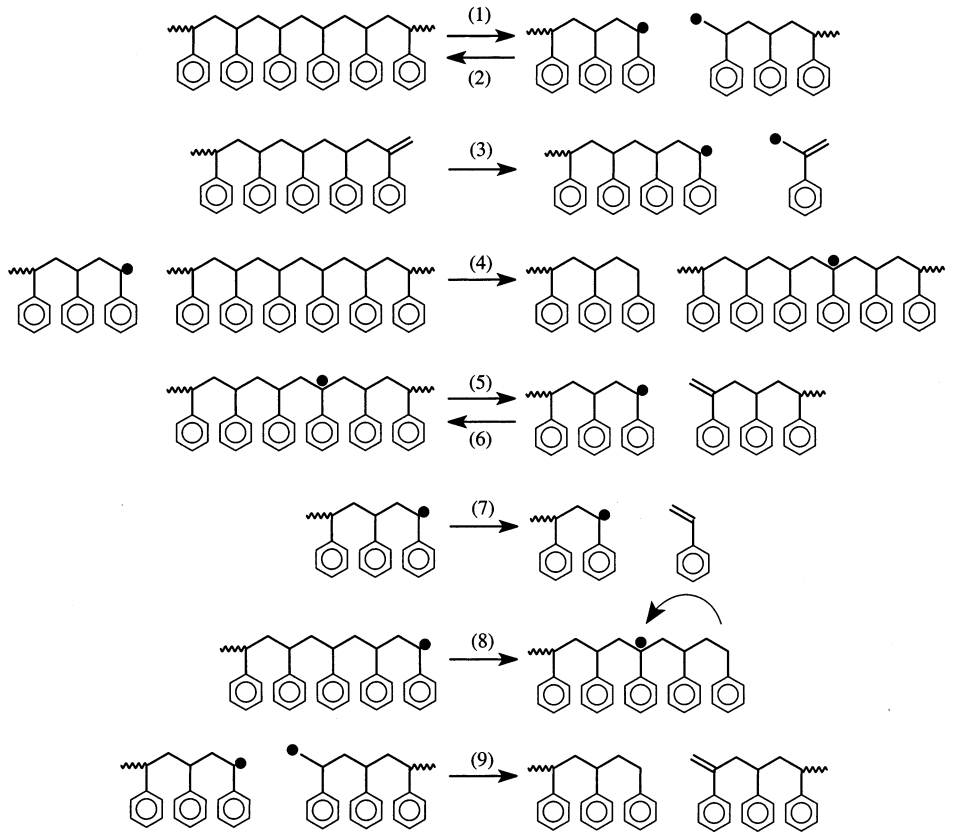


**Figure 1.** Polystyrene pyrolysis reactions incorporated into model. Reaction types are numbered in the preceding text.

in eq 4. For random fission McCoy has determined $C_m$ to be defined as shown in eq 5:[12]

$$D_n \underset{k_c}{\overset{k_f}{\leftrightarrow}} Re_i + Re_{n-i} \quad \text{(a)}$$

$$\binom{m}{j} = \frac{m!}{j!(m-j)!} \quad (1)$$

$$\frac{dD^m}{dt} = -k_f(2D^{m+1} - e_f D^m) + \frac{1}{2}k_c \sum_{i=0}^{m} \binom{m}{j} Re^j Re^{m-j} \quad (2)$$

$$D^3 = \frac{2D^2D^2}{D^1} - \frac{D^2D^1}{D^0} \quad (3)$$

$$\frac{dRe^m}{dt} = 2k_f C_m(2D^{m+1} - e_f D^m) - k_c Re^m Re^0 \quad (4)$$

$$C_m = \frac{1}{m+1} \quad (5)$$

**Moment Equations for Specific Chain Fission/ Radical Recombination.** This chain fission involves the fission of a specific carbon−carbon bond along the backbone of a polymer chain to form a low molecular weight radical as shown in reaction 3 in Figure 1. This reaction can be represented as shown in reaction b below where the low molecular weight radical produced is represented by $r_s$ and $s$ is the length of the low molecular weight radical in monomer units. Moment equations for this reaction have been developed by McCoy and coworkers[12,23] and are given in eqs 6 and 7. The low molecular weight radical concentration is monitored through eq 8.

$$D_n \underset{k_c}{\overset{k_{fs}}{\leftrightarrow}} Re_{n-s} + r_s \quad \text{(b)}$$

$$\frac{dD^m}{dt} = -k_{fs}D^m + k_c \sum_{j=0}^{m} \binom{m}{j} Re^{m-j}(s)^j [r_s] \quad (6)$$

$$\frac{dRe^m}{dt} = k_{fs} \sum_{j=0}^{m} \binom{m}{j} (-s)^j D^{m-j} - k_c Re\,[r_s] \quad (7)$$

$$\frac{d[r_s]}{dt} = k_{fs}D^0 - k_c Re^0 [r_s] \quad (8)$$

**Moment Equations for Hydrogen Abstraction.** Hydrogen abstraction involves the abstraction of a hydrogen along the backbone of a polymer chain by an end-chain radical to produce a tertiary midchain radical. This reaction is illustrated as reaction 4 in Figure 1. Hydrogen abstraction is represented by reaction c where the Rm variable represents the midchain radical produced. The moment expressions in eqs 9−11 are an extension of the expressions for chain transfer developed by Pladis and Kiparissides.[24] The variables $N_H^m$ and $N_H^e$ represent the number of abstractable hydrogen atoms per monomer unit in the middle and at the ends of the chains, respectively. The $e_t$ variable represents the number of monomer units along a polymer chain that do not undergo this general midchain hydrogen abstraction reaction (such as hydrogen on unsaturated units and chain-end units). Moment equations similar to these

were developed for the abstraction of hydrogen by lowmolecular weight radicals.

$$\mathrm{Re}_n + \mathrm{D}_i \underset{k_{\mathrm{tr,m}}}{\overset{k_{\mathrm{tr,e}}}{\leftrightarrow}} \mathrm{D}_n + \mathrm{Rm}_i \quad \text{(c)}$$

$$\frac{\mathrm{dD}^m}{\mathrm{d}t} = -N_{\mathrm{H}}{}^{\mathrm{m}} k_{\mathrm{tr,e}} \mathrm{Re}^0 (\mathrm{D}^{m+1} - e_{\mathrm{t}} \mathrm{D}^m) + N_{\mathrm{H}}{}^{\mathrm{m}} k_{\mathrm{tr,e}} \mathrm{Re}^m (\mathrm{D}^1 - e_{\mathrm{t}} \mathrm{D}^0) + N_{\mathrm{H}}{}^{\mathrm{e}} k_{\mathrm{tr,m}} \mathrm{Rm}^m \mathrm{D}^0 - N_{\mathrm{H}}{}^{\mathrm{e}} k_{\mathrm{tr,m}} \mathrm{Rm}^0 \mathrm{D}^m \quad (9)$$

$$\frac{\mathrm{dRe}^m}{\mathrm{d}t} = -N_{\mathrm{H}}{}^{\mathrm{m}} k_{\mathrm{tr,e}} \mathrm{Re}^m (\mathrm{D}^1 - e_{\mathrm{t}} \mathrm{D}^0) + N_{\mathrm{H}}{}^{\mathrm{e}} k_{\mathrm{tr,m}} \mathrm{Rm}^0 \mathrm{D}^m \quad (10)$$

$$\frac{\mathrm{dRm}^m}{\mathrm{d}t} = N_{\mathrm{H}}{}^{\mathrm{m}} k_{\mathrm{tr,e}} \mathrm{Re}^0 (\mathrm{D}^{m+1} - e_{\mathrm{t}} \mathrm{D}^m) - N_{\mathrm{H}}{}^{\mathrm{e}} k_{\mathrm{tr,m}} \mathrm{Rm}^m \mathrm{D}^0 \quad (11)$$

**Moment Equations for *β*-Scission/Radical Addition.** *β*-Scission and radical addition are represented in reaction d below. Moment equations for this reaction are similar to the equations for chain fission and are given below for the midchain radical in eq 12. Note that the midchain radical can undergo midchain *β*-scission on either side of the midchain radical, thus the factor of 2. Moment equations are shown below for the end-chain radical and the dead species formed as products in eqs 13 and 14, respectively, where $C_m$ is defined by eq 5.

$$\mathrm{Rm}_{\mathrm{n}} \underset{k_{\mathrm{ra}}}{\overset{k_{\mathrm{bs}}}{\leftrightarrow}} \mathrm{Re}_i + \mathrm{D}_{n-i} \quad \text{(d)}$$

$$\frac{\mathrm{dRm}^m}{\mathrm{d}t} = -2k_{\mathrm{bs}} \mathrm{Rm}^m + k_{\mathrm{ra}} \sum_{j=0}^{m} \binom{m}{j} \mathrm{Re}^j \mathrm{D}^{m-j} \quad (12)$$

$$\frac{\mathrm{dRe}^m}{\mathrm{d}t} = 2k_{\mathrm{bs}} C_m \mathrm{Rm}^m - k_{\mathrm{ra}} \mathrm{Re}^m \mathrm{D}^0 \quad (13)$$

$$\frac{\mathrm{dD}^m}{\mathrm{d}t} = 2k_{\mathrm{bs}} C_m \mathrm{Rm}^m - k_{\mathrm{ra}} \mathrm{Re}^0 \mathrm{D}^m \quad (14)$$

**Moment Equations for Depropagation/Propagation.** Depropagation (end-chain *β*-scission) and propagation are represented below in reaction e where M represents monomer produced. The moment equations for this reaction are similar to those for specific chain fission. The moment equations for the end-chain radical are given in eq 15, and the monomer concentration is monitored using eq 16.

$$\mathrm{Re}_n \underset{k_{\mathrm{p}}}{\overset{k_{\mathrm{dp}}}{\leftrightarrow}} \mathrm{Re} + \mathrm{M} \quad \text{(e)}$$

$$\frac{\mathrm{dRe}^m}{\mathrm{d}t} = -k_{\mathrm{dp}} \mathrm{Re}^m + k_{\mathrm{p}} \sum_{j=0}^{m} \binom{m}{j} \mathrm{Re}^{m-j} [\mathrm{M}] + k_{\mathrm{dp}} \sum_{j=0}^{m} \binom{m}{j} (-1)^j \mathrm{Re}^{m-j} - k_{\mathrm{p}} \mathrm{Re}^m [\mathrm{M}] \quad (15)$$

$$\frac{\mathrm{d[M]}}{\mathrm{d}t} = k_{\mathrm{dp}} \mathrm{Re}^0 - k_{\mathrm{p}} \mathrm{Re}^0 [\mathrm{M}] \quad (16)$$

**Moment Equations for Backbiting.** This reaction involves a radical transfer five or three carbons down a polymer chain to transform an end-chain radical into a midchain radical. This reaction is represented below in reaction f. We developed moment equations for this reaction, and these moment equations are shown in eqs 17 and 18 below.

$$\mathrm{Re}_n \underset{k_{\mathrm{bbr}}}{\overset{k_{\mathrm{bdf}}}{\leftrightarrow}} \mathrm{Rm}_n \quad \text{(f)}$$

$$\frac{\mathrm{dRe}^m}{\mathrm{d}t} = -k_{\mathrm{bbf}} \mathrm{Re}^m + k_{\mathrm{bbr}} \mathrm{Rm}^m \quad (17)$$

$$\frac{\mathrm{dRm}^m}{\mathrm{d}t} = k_{\mathrm{bbf}} \mathrm{Re}^m - k_{\mathrm{bbr}} \mathrm{Rm}^m \quad (18)$$

**Moment Equations for Specific *β*-Scission.** This reaction involves the breakage of a bond in the *β*-position to a midchain radical located at a specific location along a polymer chain. This reaction results in the production of a dead low molecular weight product and an end-chain radical, or a low molecular weight radical and a dead polymer chain. The specific *β*-scission reaction forming a dead low molecular weight product is represented in reaction g below. Moment equations for this reaction are similar to those for specific chain fission and are given in eq 19 for the midchain radical. Moment equations for the end-chain radical produced are given in eq 20, and the low molecular weight product concentration is tracked using eq 21. Equations can similarly be developed for the *β*-scission reaction resulting in the formation of a low molecular weight radical and a dead polymer chain.

$$\mathrm{Rm}_{\mathrm{n}} \underset{k_{\mathrm{ra}}}{\overset{k_{\mathrm{bs}}}{\leftrightarrow}} \mathrm{Re}_{n-s} + \mathrm{d}_s \quad \text{(g)}$$

$$\frac{\mathrm{dRm}^m}{\mathrm{d}t} = -k_{\mathrm{bs}} \mathrm{Rm}^m + k_{\mathrm{ra}} \sum_{j=0}^{m} \binom{m}{j} \mathrm{Re}^{m-j} (s)^j [\mathrm{d}_s] \quad (19)$$

$$\frac{\mathrm{dRe}^m}{\mathrm{d}t} = k_{\mathrm{bs}} \sum_{j=0}^{m} \binom{m}{j} (-s)^j \mathrm{Rm}^{m-j} - k_{\mathrm{ra}} \mathrm{Re}^m [\mathrm{d}_s] \quad (20)$$

$$\frac{\mathrm{d[d}_s]}{\mathrm{d}t} = k_{\mathrm{bs}} \mathrm{Rm}^0 - k_{\mathrm{ra}} \mathrm{Re}^0 [\mathrm{d}_s]$$

**Moment Equations for Disproportionation.** Disproportionation involves the termination of two end-chain radicals to form two dead polymer species. This reaction is represented below in reaction h. Employing the method of moments, generation and consumption terms can be formulated for the dead polymer produced and the consumption of end-chain radicals as shown in eqs 22 and 23, respectively.

$$\mathrm{Re}_n + \mathrm{Re}_i \xrightarrow{k_{\mathrm{d}}} \mathrm{D}_n + D_i \quad \text{(h)}$$

$$\frac{\mathrm{dD}^m}{\mathrm{d}t} = k_{\mathrm{d}} \mathrm{Re}^m \mathrm{Re}^0 + k_{\mathrm{d}} \mathrm{Re}^0 \mathrm{Re}^m \quad (22)$$

$$\frac{\mathrm{dRe}^m}{\mathrm{d}t} = -k_{\mathrm{d}} \mathrm{Re}^m \mathrm{Re}^0 - k_{\mathrm{d}} \mathrm{Re}^0 \mathrm{Re}^m \quad (23)$$

**Incorporating Branching.** During polymer degradation, chain fission and *β*-scission dominate the degradation pathways and lead to a dramatic decrease in the polymer molecular weight. However, chain transfer and *β*-scission lead to the formation of midchain radicals and unsaturated end-chain groups that can participate in the branching reactions illustrated in Figure 2. A small amount of branching is known to occur during

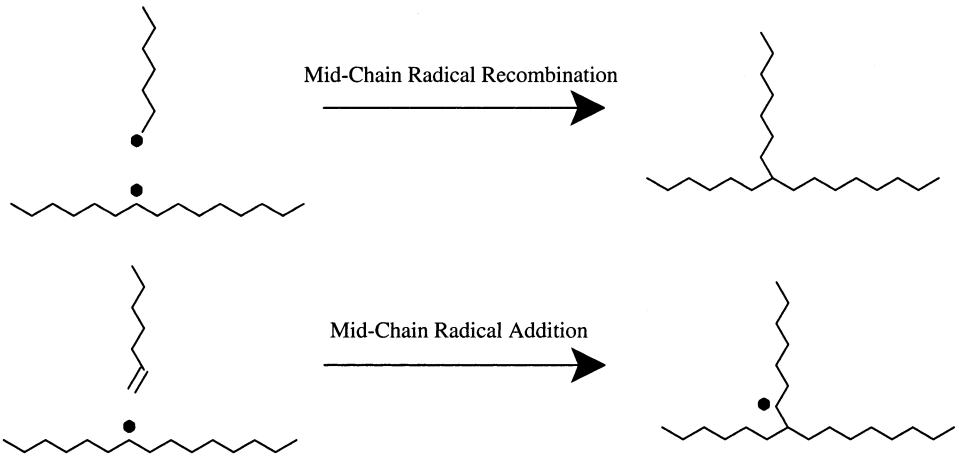


**Figure 2.** Polymer branching reactions.

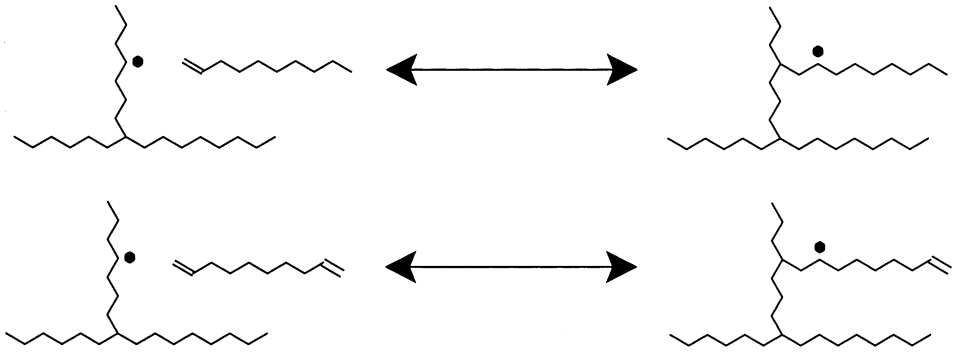

**Figure 3.** Two possible radical additions that form branches.

styrene polymerization,[29] and branching would be even more pronounced during polymer degradation due to the higher potential for the formation of midchain radicals to participate in branching reactions. Therefore, branching reactions need to be included in a polymer degradation model since a small amount of branching can affect the polydispersity of the degrading polymer mixture. However, tracking all branched species is computationally demanding, and including branched species in an approximate manner is desired. Previously, a branching method was utilized where branched species were lumped into groups with roughly no unsaturated ends, $^1/_3$ unsaturated ends, $^2/_3$ unsaturated ends, and all unsaturated ends.[1] However, with this method end-chain types are not precisely tracked, making it difficult to maintain a direct link between structure and reactivity.

A new method has been developed herein to track branching in an approximate manner while tracking end-chain types exactly. With this method, all branched species are lumped into one branched group. The branched group is then described by several properties defining the structure of the branched species. The properties tracked include end-chain types, average number of branches, and the fraction of branched species with one branch. From these properties, and by making reasonable assumptions about the structure, branching can be modeled using descriptive kinetics.

Figure 3 illustrates two reactions in which midchain radical addition leads to the addition of a branch to a branched radical. With this branching method, the addition of chain ends in these reactions is tracked, and the fact that a saturated end is added in the top reaction and an unsaturated end is added in the bottom one is taken into account. Using the end-chain types of the branched group, fractions are calculated to determine the probability of a chain end being of a specific type. These probabilities are then used to partition subsequent fission and $\beta$-scission reactions of branched species among possible outcomes. If the branched radical species in the lower reaction in Figure 3 represents the end-chain types within the branched group, where $^1/_4$ of the ends are unsaturated and $^3/_4$ are saturated, then there would be a probability of $^1/_4$ that a $\beta$-scission releasing an outer branch would release a branch with an unsaturated end. In this case, the rate of the bottom $\beta$-scission reaction illustrated in Figure 3 is partitioned between $\beta$-scission reactions releasing unsaturated ($^1/_4$) and saturated ends ($^3/_4$). In addition, by knowing the average number and types of chain ends within the branched group, the average number of branched points ($N_{br}$) can be determined from eq 24 below.

$$N_{br} = N_{ends} - 2 \tag{24}$$

The types of branches are also tracked in a fashion similar to how the types of ends are tracked, where the head−tail connectivity of the branch and whether the branch was added to a specific radical is taken into account. To allow reactions where branches break off to occur, the fraction of branched species with just one branch needs to be determined to include cases where branched species break into two linear chains. To obtain this fraction, a geometric distribution for the number of branches on a branched species was assumed. This distribution was chosen since it is believed that the fraction of chains with one, two, three, or more branches decreases in that order, so the largest fraction is the

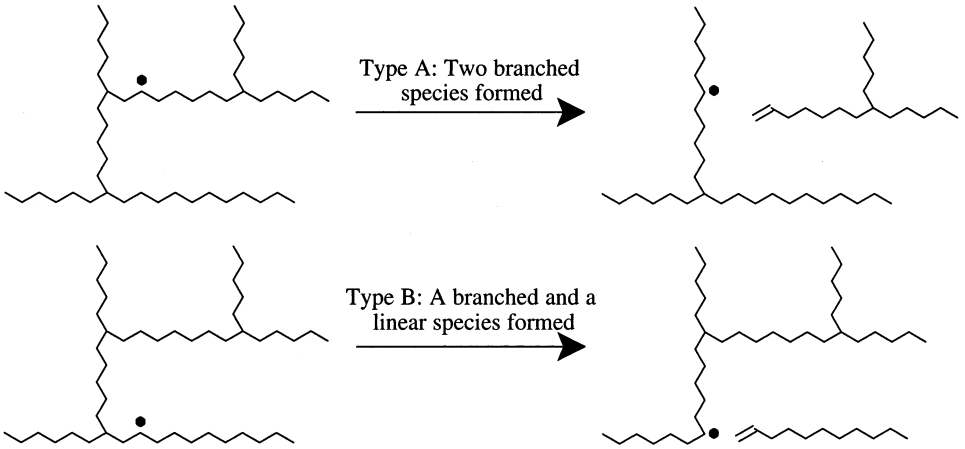


**Figure 4.** Branch point $\beta$-scission.

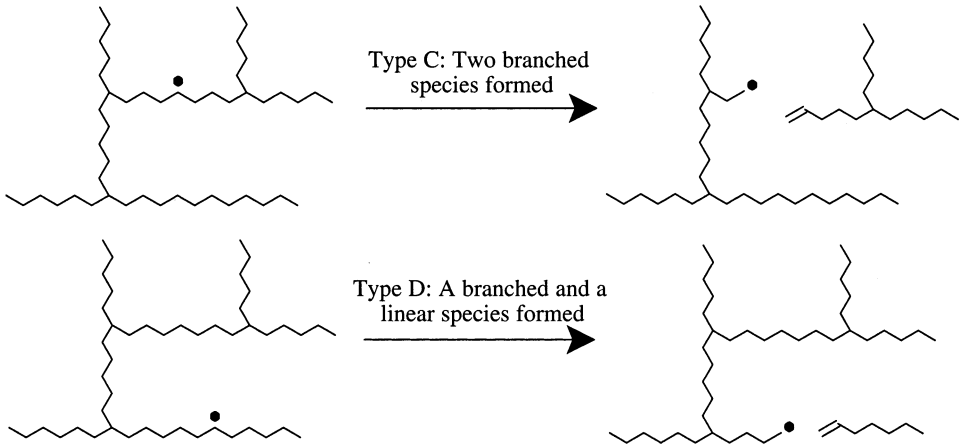


**Figure 5.** Nonbranch point $\beta$-scission.

fraction having one branch. In eq 25 below, $F_n$ represents the probability of a branched chain having $n$ branches, and $p$ represents the probability that a branched chain chosen at random has an additional branch.

$$F_n = p^{n-1}(1-p) \tag{25}$$

$$F_1 = (1-p) \tag{26}$$

With the average number of branches known from eq 24, the value of $p$ in eq 25 can be determined from eq 27 below by setting the expectation for the average number of branches equal to the average number of branches from eq 24.

$$p = 1 - \frac{1}{N_{\mathrm{br}}} \tag{27}$$

Next, different types of branch fission and $\beta$-scission reactions have to be taken into account. Around each branch point there are three possible breakage points. If it is assumed that all the branches added to a branched species are added to the outer limbs (which is reasonable based on steric arguments), then the probability of breaking a branch at a branch point and releasing a linear species can be calculated. The probabilities shown in eqs 28 and 29 have been determined for the two types of $\beta$-scission reactions shown in Figure 4 (these probabilities also apply to fission at branch points). The fractions calculated with eqs 28 and 29 are multiplied by the overall rate of $\beta$-scission at branch points to partition the rate between possible outcomes. The type of branched midchain radical shown in Figure 4 is distinguished from typical midchain branched radicals where $\beta$-scission does not break a branch. In actuality, some of these $\beta$-scission reactions could produce linear midchain radicals, but due to difficulties in model solution if this case was accounted for specifically, this possibility is lumped into the fraction resulting in two branched species.

Type A: $$p_{\mathrm{A}} = 2\frac{N_{\mathrm{br}} - 1}{3N_{\mathrm{br}}} \tag{28}$$

Type B: $$p_{\mathrm{B}} = 1 - p_{\mathrm{A}} \tag{29}$$

Next, fission and $\beta$-scission can occur at places other than branch points as shown in Figure 5. For the two cases illustrated in Figure 5, probabilities have been derived assuming that branches are only added to outer limbs, branches add to the middle of limbs, and all limbs are of equal size. The probabilities are given in eqs 30 and 31, and these $\beta$-scission reactions involve typical midchain radicals tracked separately from the branched midchain radicals that undergo type A and B $\beta$-scission. Similar to eqs 28 and 29, the fractions calculated by eqs 30 and 31 are multiplied by the overall rate of $\beta$-scission of typical midchain branched radicals to partition the rate between possible outcomes. Equations 30 and 31

are also applied to nonbranch point chain fission where the three bonds around branch points are excluded.

Type C: $$p_C = \frac{N_{br} - 1}{2(N_{br} + 2)} \quad (30)$$

Type D: $$p_D = 1 - p_C \quad (31)$$

Finally, partitioning the mass of a degrading branched species between possible products needs to be properly managed. It has been shown that the fission and $\beta$-scission of branched chains favor the formation of long and short fragments.[30] McCoy and co-workers[12,18] have developed methods for describing both random and proportioned fission, but with the decomposition of branched species, a mix of random and proportioned fission is required to produce long and short fragments simultaneously. The methods developed by McCoy and co-workers were extended here to develop new stoichiometric coefficients describing the fission of branched chains. For type B and D $\beta$-scission (or fission) illustrated in Figures 4 and 5, it is assumed that the size of the branch released can vary randomly between twice the average size of a limb and zero. The larger branched species remaining can vary between the full size down to the full species' size minus the size of two limbs. By defining the size limits in this manner, the stoichiometric coefficient can be determined for the rate of formation of the two products. Equations 32 and 33 below represent the moment equations for the rate of formation of the linear and branched products, respectively. The variable $f$ equals twice the average size of a limb divided by the full size of the branched species.

$$\int_0^\infty \int_0^{fy} x^m k_{fb} D_y \frac{1}{fy} dx\, dy = k_{fb}\left[\frac{f^m}{(m+1)}\right] D^m \quad (32)$$

$$\int_0^\infty \int_{(1-f)y}^{y} x^m k_{fb} D_y \frac{1}{fy} dx\, dy = k_{fb}\left[\frac{1}{f(m+1)} - \frac{(1-f)^{m+1}}{f(m+1)}\right] D^m \quad (33)$$

For type A and C $\beta$-scission (or fission) illustrated in Figures 4 and 5, it is assumed that the size of the two branched species can vary between the average size of a branch and the full length minus the average length of one branch. The common fraction $f$ for this case is the average size of a branch divided by the full size of the branched species, and using this fraction the stoichiometric coefficients can be determined. Equation 34 below represents the moment equations for the rate of formation of each branched product.

$$\int_0^\infty \int_{fy}^{(1-f)y} x^m k_{fb} D_y \frac{1}{(1-2f)y} dx\, dy = k_{fb}\left[\frac{(1-f)^{m+1} - f^{m+1}}{(m+1)(1-2f)}\right] D^m \quad (34)$$

**Specification of Rate Constants.** Incorporation of these free radical elementary step reactions in a model of polymer degradation requires specification of the rate parameters. The same approach used previously in our work to quantify rate constants was adopted.[2] The rate parameters were dependent on not only the reaction type but also the structural characteristics of the reactants and products. Assuming the validity of the Arrhenius relationship, it was necessary to specify a frequency factor and an activation energy for each reaction. Each reaction of a given type (e.g., bond fission) shared the same frequency factor.

To establish a link between the structure of the reactants and products and the elementary step rate constant, the activation energy was described using the Evans−Polanyi relationship,[31] in which the activation energy is related linearly to the heat of reaction, i.e., $E = E_0 + \alpha\Delta H_R$. The values of the heats of reaction were obtained from experimental polymerization data or based on analogous reactions of molecular mimics of the polymer structure as used previously.[2,3] The primary method by which the heats of reaction were calculated was the Structures and Properties Database from the National Institute of Standards.[32]

Termination reactions are known to be diffusion-controlled,[33] and to implement the appropriate diffusion dependence on chain length for termination reactions, a simplified form of Smoluchowski's equation[34] for the rate constant of a diffusion-controlled reaction was used. The resulting dependence of the termination rate constant on chain length is given in eq 35 below.

$$k_t = k_t^o\left(\frac{1}{i^\gamma} + \frac{1}{j^\gamma}\right)/2 \quad (35)$$

In eq 35, $k_t^o$ represents the termination rate constant for two end-chain radicals of length one, $i$ and $j$ represent the chain lengths in monomer units of the terminating radicals, $\gamma$ represents the diffusion dependence on chain length, and $k_t$ represents the termination rate constant used in termination rate expressions. The Rouse model[35] gives a diffusion dependence that is inversely proportional to the chain length ($\gamma = 1$) and has been shown to work well for diffusion in bulk polymer below the entanglement limit.[36] However, for chains above the entanglement limit, a more appropriate reptation model[33,37] gives a diffusion dependence that is inversely proportional to the chain length squared ($\gamma = 2$). Within the polymer degradation model developed, a value of $\gamma$ was chosen to be one or two based on whether the average size of the polymer chains was mostly above or below the entanglement limit during the degradation time frame. In addition, a value of $k_t$ was calculated for all termination reactions using an $i$ and $j$ averaging in the lengths of all the polymer radicals present in the polymer melt.

Next, chain transfer has been found to depend on the polymer chain length. Using collision theory, it has been shown that the chain transfer rate constant should be inversely proportional to the size of the abstracting radical.[38] Equation 36 has been incorporated into the model to account for this effect, where $i$ represents the length of the end-chain radical involved in the chain transfer reaction and $k_{tr}^o$ represents the chain transfer rate constant for a radical chain length of 1.

$$k_{tr} = k_{tr}^o\left(\frac{1}{i}\right) \quad (36)$$

**Model Assembly and Solution.** Because of the large number of species and reactions, a program was developed to construct a list of the chemical reactions in traditional form. A parsing grammar was then developed which could transform this list into population-balance equations. Perl scripts implemented appropriate rules for transforming elementary reactions to population-balance equations, and moment opera-

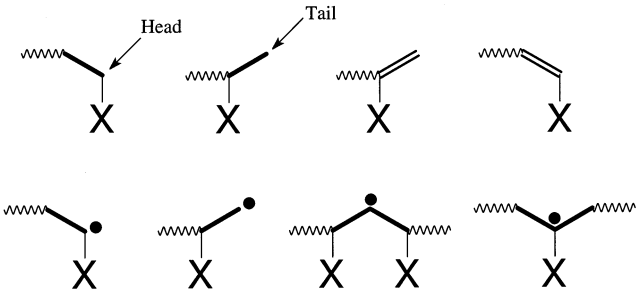


**Figure 6.** End-chain and radical structures in polymeric species. The "X" represents the substituent group.

**Table 1. Number of Structures Tracked Determining the Number of Species Tracked**

| | | | |
|---|---|---|---|
| head/tail distinguished | no | no | yes |
| saturated/unsaturated distinguished | no | yes | yes |
| no. of linear dead chains | 1 | 3 | 10 |
| no. of linear midchain radicals | 1 | 3 | 10 (tail mid)<br>10 (head mid) |
| no. of linear end-chain radicals | 1 | 2 | 4 (tail end)<br>4 (head end) |

tions were automatically invoked to transform these reactions into terms of the moment equations for each species. These terms were then assembled into a set of ordinary differential equations that included three (zeroth, first and second) moment equations for each unique species. The third moments of unique dead polymeric species were estimated using an approximation developed previously[28] which has been shown to approximate the true third moment very accurately for unimodal distributions with a polydispersity between 1.5 and 2.5.[39] The resultant set of stiff differential equations was then solved using DASSL.[40]

To choose what polymer species were to be tracked, a lumping scheme was devised. In the moment equations shown previously, all dead polymer, end-chain radicals, and midchain radicals were lumped into the groups labeled D, Re, and Rm, respectively. This is the simplest lumping scheme since only three types of polymeric species are tracked explicitly. However, there are different types of end-chain groups and different types of radicals possible as shown in Figure 6 where the "X" represents the substituent group. Table 1 shows how the model size grows considerably as more end-chain and radical features are tracked, which subsequently requires more moment equations to track the different polymeric species.

With the program developed, which initially produces a list of chemical reactions, the types of features to be tracked are specified and the reactions are output accordingly. For polystyrene, the phenyl group on the head end of a monomer unit provides resonance stabilization for any radical, and therefore its reactivity must be distinguished from tail ends. In addition, unsaturated groups have different reactivities and participate in different reactions (such as radical addition) compared to saturated end-chain groups, so they also must be tracked accordingly. Therefore, to model polystyrene, both head and tail ends, saturated and unsaturated, were differentiated in the model developed.

In addition, the model tracks structural irregularities within polymer chains. When head and tail ends are tracked separately, all atypical bonds (tail−tail and head−head) are tracked explicitly in a fashion similar to how the ends of branched species are tracked. Using the concentrations of the different types of bonds, probabilities were incorporated into the model to partition fission reactions between possible breaking bonds where different heats of reaction are used to characterize each possible bond fission reaction. Tracking these atypical bonds is necessary for polystyrene where the recombination of end-chain head polystyrene radicals produces weak links within polymer chains. All polystyrene samples degraded were assumed to lack these links initially since the nature of the propagation process and the stringent purity requirements for the monomer and solvent limit the possibility of abnormality formation during anionic polymerization.[41]

## Experimental Section

Batch pyrolysis experiments were carried out by reacting 10−20 mg polystyrene samples. The 5160, 98 100, and 50 550 molecular weight polystyrene samples were anionically polymerized as previously described.[2,3] The 42 500 molecular weight polystyrene was a narrow polystyrene standard obtained from Scientific Polymer Products Inc. Samples were loaded into 3 mL glass ampules (Wheaton), purged with argon for 2 min, and flame-sealed. Because of the small loadings, only 0.3% of the volume of the ampules consisted of polystyrene. This kept the pressure in the gas-phase low during the pyrolysis experiments (<5 bar) even though volatile low molecular weight products were being evolved. Gas-phase reactions were minimized due to the low concentration of the low molecular weight products in this phase. Samples were thermally degraded by suspending the ampules for a series of reaction times ranging from 5 to 180 min in an isothermal fluidized sandbath at 310−420 °C. After removal from the high temperature sandbath, the ampules were cooled to room temperature in another fluidized sandbath at room temperature.

To analyze the full molecular weight range of products observed from the polymer pyrolyses, three complementary analytical techniques were used:[2,3] gel permeation chromatography (GPC), gas chromatography (GC), and gas chromatography−mass spectroscopy (GC−MS). GPC was used to monitor the temporal evolution of the high molecular weight products, while the identification and quantification of the low molecular weight products were performed using GC and GC−MS. First, 2.0 mL of HPLC grade methylene chloride (Aldrich) was used to dissolve each degraded sample, and the product solution was agitated by shaking the vessel and then injected into a vial using a glass syringe (Fisher) and a 0.45 $\mu$m polypropylene filter (Alltech). The solution was next injected into a Waters gel permeation chromatograph equipped with a Waters 510 pump, 717 plus autosampler, 410 differential refractometer, a column heater module containing three (HR 1, 2, and 4) Styragel 5 $\mu$m particle columns with dimensions of 7.8 × 300 mm, and a fraction collector. The low molecular weight fraction (<400 amu) of the GPC eluant was collected with the fraction collector, and biphenyl was used as an external standard. For quantification, standard solutions containing some of the major reaction products or compounds of similar size (toluene, styrene, α-methylstyrene (Aldrich), and 2,4-diphenyl-4-methyl-1-pentene (α-methylstyrene dimer)) were also prepared. The reaction products were identified with an HP 6890 Series gas chromatograph with an HP-5MS 5% phenyl methyl siloxane capillary column (30.0 m × 250 $\mu$m × 0.25 $\mu$m nominal) and equipped with a mass selective detector (GC−MS). Decomposition products were quantified with an HP 6890 Series gas chromatograph equipped with a flame ionization detector and the same type of capillary column. The error bars shown in the figures in this paper represent the standard deviations of experiments, which were all performed in triplicate.

## Polystyrene Pyrolysis Modeling

A summary of the frequency factors, Evans−Polanyi constants, and heats of reaction for the main degradation reactions for polystyrene is provided in Table 2.

**Table 2. Representative Values of Kinetic and Thermodynamic Parameters for Reaction Types Incorporated into a Mechanistic Model of Polystyrene Degradation**

| reaction type | frequency factor, $A$ ($s^{-1}$ or l $mol^{-1}$ $s^{-1}$) | intrinsic barrier, $E_o$ (kcal $mol^{-1}$) | α, transfer coeff | representative heat of reaction (kcal $mol^{-1}$) | activation energy (kcal $mol^{-1}$) |
|---|---|---|---|---|---|
| chain fission | $1.0 \times 10^{16}$ | 2.3[c] | 1.0 | 65.0[i] | 67.3 |
| chain fission allyl | $5.5 \times 10^{13}$ [a] | 2.3[c] | 1.0 | 55.0 | 57.3 |
| radical recombination | $1.1 \times 10^{11}$ [b] | 2.3[c] | 0.0 | −65.0[i] | 2.3 |
| disproportionation | $5.5 \times 10^{9}$ [d] | 2.3[c] | 0.0 | | 2.3 |
| end-chain β-scission | $4.1 \times 10^{12}$ [f] | 11.4[e] | 0.76 | 17.5[f] | 24.7 |
| midchain β-scission | $4.1 \times 10^{12}$ [f] | 11.4[e] | 0.76 | 22.0 | 28.1 |
| radical addition | $1.5 \times 10^{7}$ [e] | 11.4[e] | 0.24 | −22.0 | 6.1 |
| hydrogen abstraction | $2.1 \times 10^{6}$ [g] | 12.0[g] | 0.30−0.70[j] | −3.1 | 10.5 |
| 1,5-hydrogen transfer | $5.0 \times 10^{6}$ [h] | 12.0 | 0.30−0.70[j] | −3.1 | 10.5 |
| 1,3-hydrogen transfer | $4.5 \times 10^{11}$ [h] | 25.0 | 0.30−0.70[j] | −3.1 | 23.5 |

[a] Frequency factor calculated from transition state theory.[42] [b] Frequency factor from data on the termination of 1-ethyl-2-phenyl radicals.[43] [c] Intrinsic barrier determined from polystyrene termination rate constants.[44] [d] Disproportionation estimated to be 5% of recombination rate from Schreck et al., 1989.[45] [e] Frequency factor and intrinsic barrier from Deady et al., 1993.[46] [f] Frequency factor backed out from equilibrium data.[47] [g] Parameters obtained from Gregg and Mayo, 1947.[48] [h] Estimated from data obtained by Kim et al., 1999.[49] [i] Bond strength for polystyrene from Aguado and Serrano, 1999.[10] [j] Calculated using the Blowers and Masel equation.[50]

Note that no optimization of the frequency factors or activation energies was carried out. Some of these values were taken directly from our previous work.[2−4] The frequency factors for allyl chain fission,[42] β-scission,[47] and radical addition[46] and the rate parameters for radical recombination and disproportionation[43−45] were obtained from the literature. However, radical recombination and disproportionation are known to be diffusion-controlled,[33] and the termination parameters in Table 2 are for a chain length of one. For longer chains, eq 35 was used to obtain the radical recombination or disproportionation rate constant. For all PS models, $\gamma$ in eq 35 was set equal to 1 since the polystyrene investigated was mostly below the entanglement limit during the degradation time frames modeled. The rate parameters for polystyrene chain transfer were obtained from data on polystyrene chain transfer with ethylbenzene (one monomer unit long).[48] Equation 37 was used within the model to obtain the polymer chain transfer rate for long chains. In addition, the rate parameters for 1,5-hydrogen transfer and 1,3-hydrogen transfer were obtained by matching the model results to the ratio of trimer to dimer (3:7) and dimer to monomer (1:4) for the pyrolysis of polystyrene in an open system at 400 °C.[49]

The full model developed for polystyrene consisted of over 2700 reactions and tracked 64 species. Within the model, head and tail chain ends were discriminated as shown in Figure 6, where the "X" represents the phenyl substituent for polystyrene. On the basis of the anionic polymerization procedure[2,3] followed to make most of the polystyrene samples degraded, the initial polystyrene structure was assumed to consist of linear chains with saturated tail ends. Only midchain head radicals were allowed due to the resonance stabilization the phenyl substituent provides. Specific midchain radicals formed from backbiting reactions were tracked separately from other midchain radicals. Branching was regulated by only allowing linear chains to add as branches to branched species. As the branched species themselves degraded the average branch length dropped to only a few monomer units long, and it was assumed these short branches would interfere with the addition of branches from other branched species.

Because polystyrene low molecular weight products below 300 amu are volatile at the reaction conditions employed in our batch pyroylsis experiments (<5 bar and 310−420 °C), they were assumed to evaporate immediately and not interact further with the degrading polymer melt. Trimer, which has a boiling point around 350 °C at atmospheric pressure, was assumed to remain in the melt for all model runs at or below 350 °C. Low molecular weight radicals, however, were assumed to react within the polymer melt before evaporating. Semibatch reactor equations were employed to track the volume shrinkage of the polymer melt as low molecular weight products were evolved. Further transformations among species partitioned into the gas phase were not incorporated into the models.

The model results in comparison to experimental data for the degradation of low molecular weight polystyrene ($M_n = 5160$; $M_w = 5850$) at 350 °C are shown in Figure 7. The results for the total $M_n$ and $M_w$ are quite similar to the experimental data, while the model results for polymer $M_n$ and $M_w$ are lower than the experimental data during the later stages of the degradation. These discrepancies are likely due to difficulties in separating the degrading polymer GPC peak from the GPC peaks of low molecular weight products. Significant overlap of these peaks occurs for the degradation of low molecular weight polystyrene. The model results for styrene, dimer, and timer yields (the three products produced in the highest quantity) and the total yield of low molecular weight products (LMWP) below 315 amu agree very well with the experimental data.

The marked separation of total $M_n$ and $M_w$ apparent in Figure 7a demands the formation of high molecular weight species concomitant with the production of low molecular weight products. The majority of this separation is the result of the end-chain β-scission rate being fast compared to the hydrogen abstraction rate, which favors the production of low molecular weight products over the breaking of chains via midchain β-scission. However, it was found that branching was significant and helped to mimic the full separation in the total $M_n$ and $M_w$.[1] While experimental and our model results (not shown) demonstrate that branching is minimal for styrene polymerization, midchain radicals are readily produced during degradation due to the abundance of abstractable midchain hydrogens on dead polystyrene chains within the melt. This leads to higher rates of branching. Branching occurs as chain-end double bonds, produced from the β-scission of midchain radicals, attach to midchain radicals forming large branched species. A small amount of branching was found to significantly affect the model results, where the mean number of branches on branched species never exceeded 2.0, and branched species always comprised less than

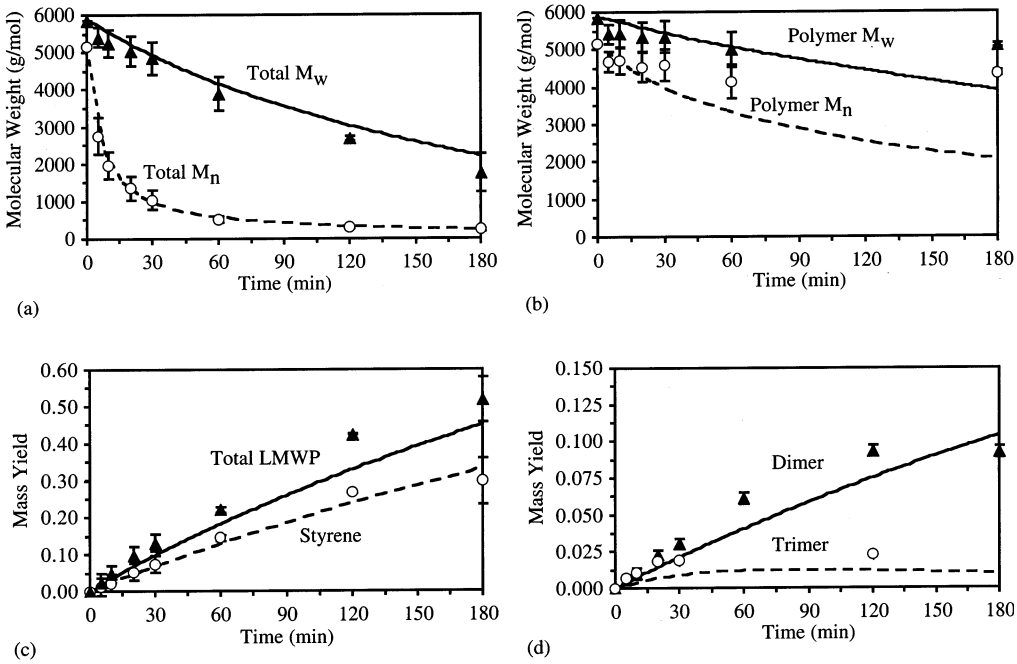


**Figure 7.** Comparison of results of model with experimental data for 5160 molecular weight polystyrene at 350 °C for (a) total $M_n$ and $M_w$, (b) polymer $M_n$ and $M_w$, (c) styrene yield and total low molecular weight product (LMWP) yield, and (d) dimer and trimer yields.

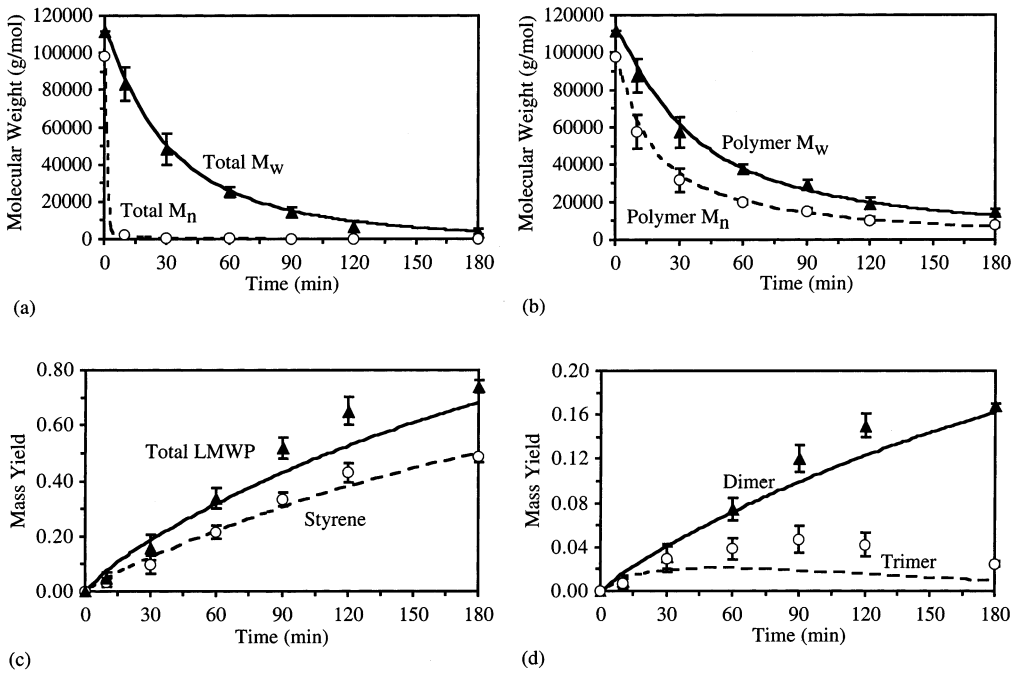


**Figure 8.** Comparison of results of model with experimental data for 98 100 molecular weight polystyrene at 350 °C for (a) total $M_n$ and $M_w$, (b) polymer $M_n$ and $M_w$, (c) styrene yield and total low molecular weight product (LMWP) yield, and (d) dimer and trimer yields.

30 wt % of the degrading polystyrene melt during all polystyrene model runs.

To show the ability of the model to handle the degradation of polystyrene samples of different molecular weights, model results in comparison to experimental data for high molecular weight polystyrene ($M_n$ = 98 100; $M_w$ = 111 800) at 350 °C are shown in Figure 8. All the model results in Figure 8 are in very good agreement with the experimental data. The trimer yield is a bit lower than the experimental yield, but some error in the trimer yield is expected since trimer has a boiling point around 350 °C at atmospheric pressure. Therefore, a significant quantity of the trimer is likely entering the gas phase during the degradation process. Within the model runs at 350 °C, trimer is assumed to remain in the polymer melt where it can participate in radical addition reactions, but if some trimer enters the gas phase, its full participation in radical addition reactions would be subdued. Therefore, a higher peak trimer yield in the experimental data is expected and was observed at 350 °C.

A sensitivity analysis on the rate parameters was performed for the model results in Figure 8 at 20 min. It was found that doubling the rate constants for any

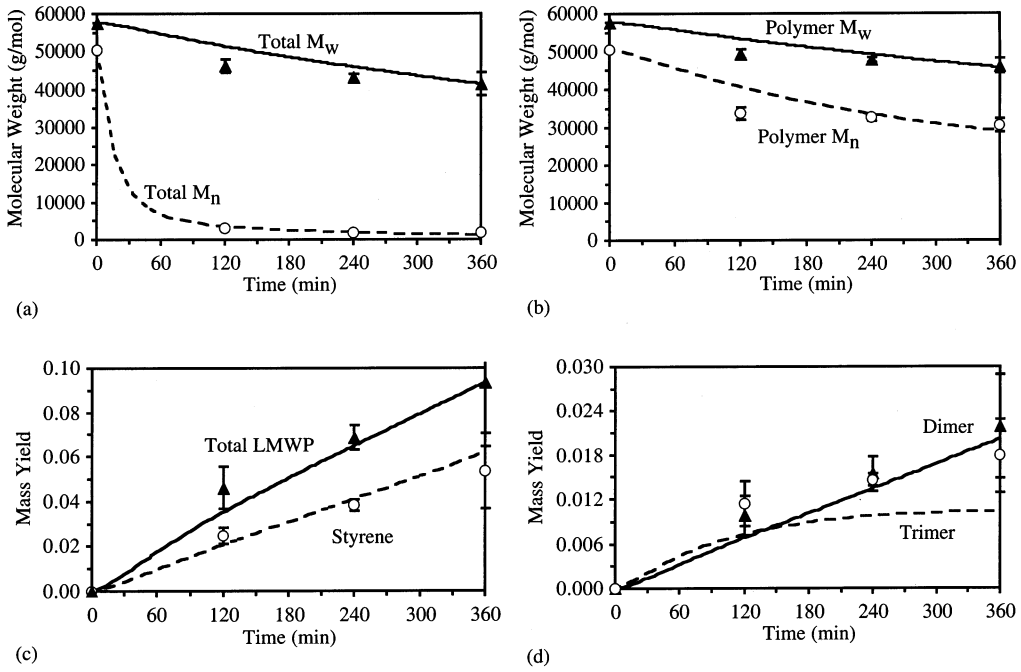


**Figure 9.** Comparison of results of model with experimental data for 50 550 molecular weight polystyrene at 310 °C for (a) total $M_n$ and $M_w$, (b) polymer $M_n$ and $M_w$, (c) styrene yield and total low molecular weight product (LMWP) yield, and (d) dimer and trimer yields.

reaction family in Table 2 (either by doubling the frequency factors or lowering the intrinsic barriers by 0.86 kcal/mol at 350 °C), except for the allyl chain fission reaction family, resulted in at least a 10% change in the styrene yield, dimer yield, trimer yield, polymer $M_n$, and polymer $M_w$ at 20 min. The styrene yield is most sensitive to chain fission and $\beta$-scission, where doubling the rate constants for these reactions resulted in a 50% and 100% increase in the styrene yield, respectively. The polymer $M_n$ and polymer $M_w$ are most sensitive to chain fission and chain transfer, where doubling the rate constants for these reactions resulted in 30% and 20% decreases in the polymer $M_n$ and polymer $M_w$, respectively. Because of the high sensitivity of the model results in Figure 8 to nearly all of the rate parameters, it is necessary to obtain the correct rate parameters to model both the evolution of the molecular weight distribution and the yields of low molecular weight products simultaneously.

To show the ability of the model to predict the degradation of polystyrene over a large temperature range, model results in comparison to experimental data for polystyrene at 310 °C ($M_n$ = 50 550; $M_w$ = 57 640), 350 °C ($M_n$ = 50 550; $M_w$ = 57 640), 380 °C ($M_n$ = 42 500; $M_w$ = 43 400), and 420 °C ($M_n$ = 98 100; $M_w$ = 111 800) are shown in Figures 9−12, respectively. The degradation rates for polystyrene differ by more than 2 orders of magnitude over this 110 °C temperature range. Overall, the model results are in very good agreement with the experimental data over this temperature range. For the modeling results at 420 °C, a warm-up time of 55 s was estimated by extrapolating the total yield of low molecular weight products to zero conversion. This warm-up period was incorporated into the model results because it was a significant fraction of the degradation time frame of interest. However, even with this warm-up time incorporated into the results, the predicted yields of low molecular weight products at 420 °C are a bit higher than the experimental trends. In addition, a sensitivity analysis on the rate parameters was performed with the model results in Figure 11 at 5 min (the yield of styrene after 5 min at 380 °C is similar to the yield of styrene after 20 min at 350 °C). It was found that the sensitivity of these model results at 380 °C to the rate parameters was almost identical to the sensitivity results presented earlier at 350 °C, indicating that small changes in the rate parameters have similar effects on model results over the temperature range investigated.

All of the experimental data at 350 °C depict a slight drop in the styrene and dimer yields at long degradation times that is not predicted by the model. This is most noticeable for the results in Figure 10, where the experimental styrene and dimer yields actually seem to level off and begin declining. To probe the behavior of styrene at longer degradation times, we performed experiments where styrene monomer was loaded into an ampule in amounts comparable to those that would be observed in the gas phase during the polystyrene degradation experiments performed. The contents were then pyrolyzed at 350 °C to determine whether styrene was reacting with itself in the gas phase to form other products. After 2 h, about 20% of the styrene had been converted to other low molecular weight products—primarily dimer, 1,3-diphenylpropane, α-methylstyrene, and toluene.

During the polystyrene degradation experiments performed at 350 °C, the formation of 1,3-diphenylpropane, α-methylstyrene, and toluene is concomitant with the slight drop of the yields of styrene and dimer observed at long degradation times. These gas phase reactions are likely similar in nature to the reactions associated with the thermal initiation of sytrene,[51] but due to their complexity and small significance in our experiments performed to moderate conversions, these reactions are not included in the model. As a result, however, the model predictions for the yields of 1,3-diphenylpropane, α-methylstyrene, and toluene are poor at long degradation times. To minimize these reactions, a semibatch reactor where styrene, dimer, and trimer are removed

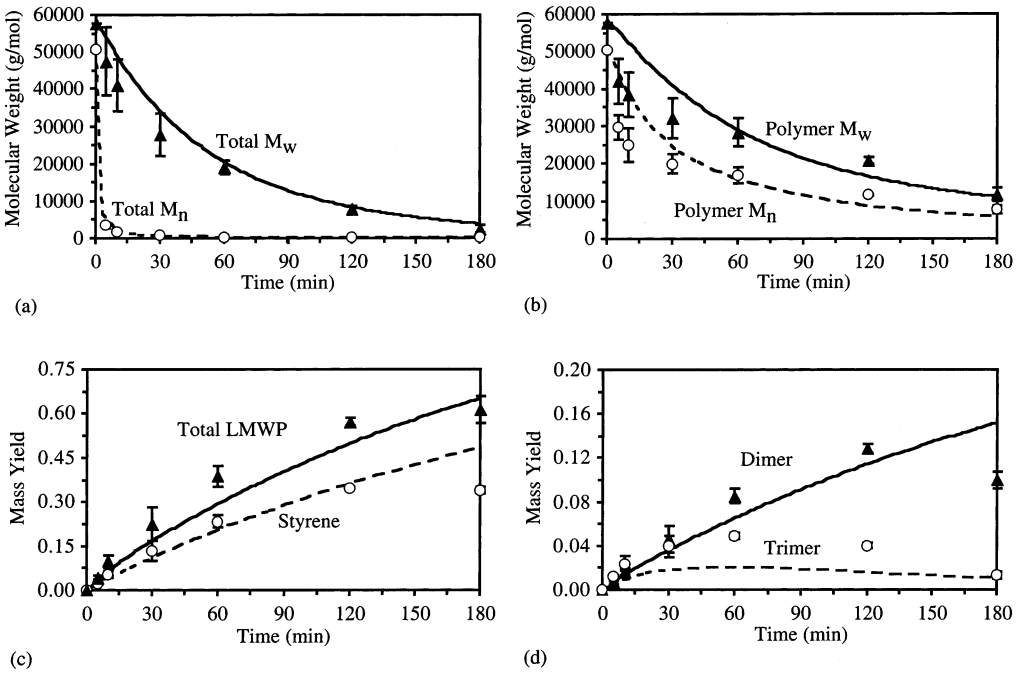


**Figure 10.** Comparison of results of model with experimental data for 50 550 molecular weight polystyrene at 350 °C for (a) total $M_n$ and $M_w$, (b) polymer $M_n$ and $M_w$, (c) styrene yield and total low molecular weight product (LMWP) yield, and (d) dimer and trimer yields.

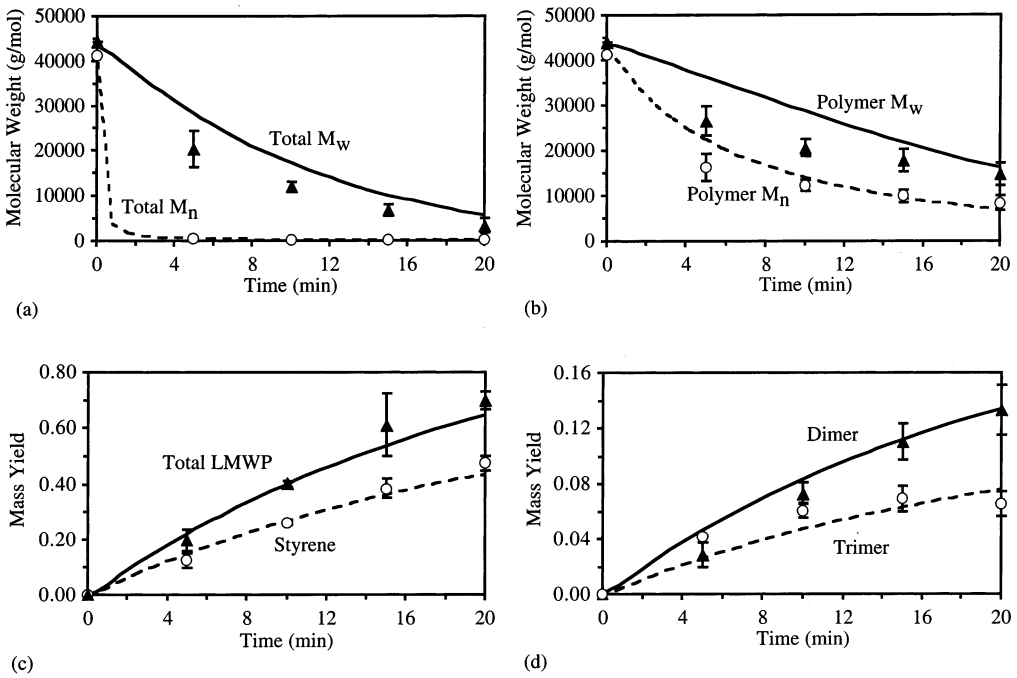


**Figure 11.** Comparison of results of model with experimental data for 42 500 molecular weight polystyrene at 380 °C for (a) total $M_n$ and $M_w$, (b) polymer $M_n$ and $M_w$, (c) styrene yield and total low molecular weight product (LMWP) yield, and (d) dimer and trimer yields.

to prevent further transformations in the gas phase is optimal. Such a reactor has been employed to degrade polystyrene at high temperatures,[52] and the degradation products at 590 °C consisted almost entirely of styrene, dimer, and trimer.

Model results are compared to isothermal thermogravimetry data reported by Bouster et al.[53] in Figure 13 and data obtained from an open batch reactor reported by Kim et al.[49] in Figure 14. The two data sets differ in their initial molecular weights (100 000 for Bouster and 222 000 for Kim) and the temperature ranges investigated (331−370 °C for Bouster and 370−400 °C for Kim). A warm-up period of 15 min was reported by Bouster, and this warm-up period was incorporated into the model results. For the data reported by Kim, some degradation of the polystyrene occurred during the warm-up period, and the model results were adjusted to match the model yield and the experimental yield at the beginning of the isothermal experiments. The model results are in good agreement with the experimental data (yield of LMWP below 315 amu) as shown in Figures 13 and 14, demonstrating the ability of the model to predict the overall degradation

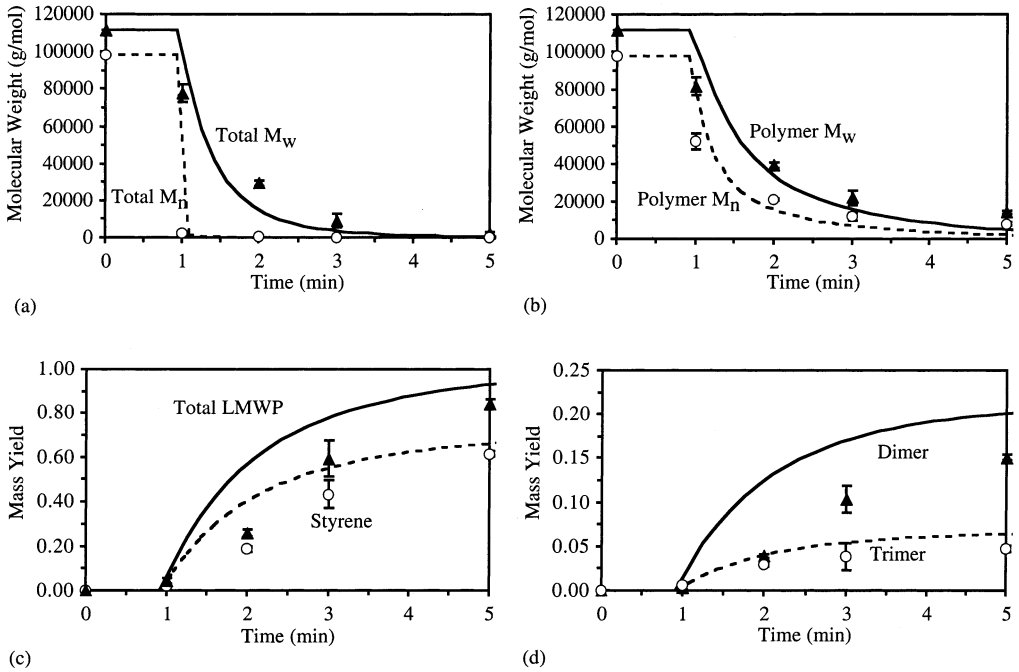


**Figure 12.** Comparison of results of model with experimental data for 98 100 molecular weight polystyrene at 420 °C for (a) total $M_n$ and $M_w$, (b) polymer $M_n$ and $M_w$, (c) styrene yield and total low molecular weight product (LMWP) yield, and (d) dimer and trimer yields.

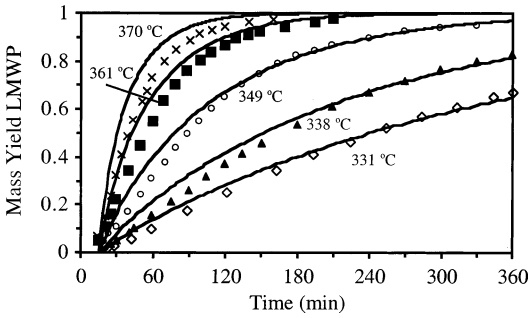


**Figure 13.** Comparison of results of model with experimental data in the literature[53] for 100 000 molecular weight polystyrene at 331−370 °C for total low molecular weight product (LMWP) yield.

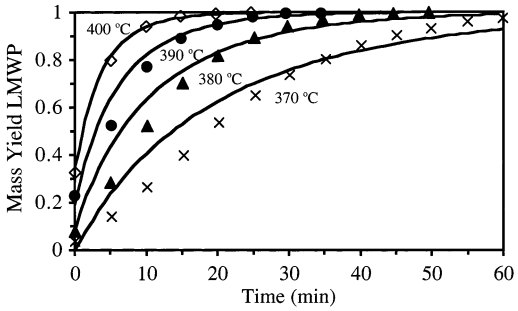


**Figure 14.** Comparison of results of model with experimental data in the literature[49] for 222 000 molecular weight polystyrene at 370−400 °C for total low molecular weight product (LMWP) yield.

rate of polystyrene in different experimental systems and at different thermal conditions.

## Conclusions

Overall, the detailed mechanistic modeling of the degradation of high molecular weight polymers is possible using population balances and the method of moments. A model was developed that included over 2700 reactions and tracked 64 species. The model incorporated a finite number of reaction types characterizing free radical polymerization and decomposition: (1) chain fission, (2) radical recombination, (3) allyl chain fission, (4) hydrogen abstraction, (5) midchain $\beta$-scission, (6) radical addition, (7) end-chain $\beta$-scission, (8) 1,5-hydrogen transfer (also 1,3-transfer), and (9) disproportionation. Polymer species were lumped into various classes to track the presence and location of radical centers, the position of double bonds, the inclusion of branches, and the orientation of the "head" and "tail" ends of the monomer units. To establish a link between the structure of the reactants and products and the elementary step rate constant, the activation energy was described using the Evans−Polanyi relationship. In addition, structural irregularities within polymer chains, such as head−head and tail−tail linkages, were tracked. The ability of the model to predict the evolution of $M_n$ and $M_w$, and the yields of styrene, dimer, and trimer over a 110 °C temperature range and for different initial polymer molecular weights was shown. Incorporating chain-length-dependent rate parameters for termination and chain transfer reactions allowed the model to handle different initial molecular weights effectively. The general modeling framework established will be extended to other single component and multicomponent polymeric systems in future work.

**Acknowledgment.** This work was supported by the MRSEC program of the National Science Foundation (DMR-9632472) at the Materials Research Center of Northwestern University and the CAREER Program of the National Science Foundation (CTS-9623741). Funding was also provided through a National Science Foundation Fellowship (T.M.K.).

## Nomenclature

A frequency factor, $s^{-1}$ or L/(mol s)

$C_m$ stoichiometric coefficient for partitioning mass between degradation products
$D^m$ $m$th moment of dead chains, mol/L
$D_n$ dead chain of length $n$
$e_f$ number of bonds not able to undergo bond fission
$e_t$ number of monomer units without abstractable midchain hydrogen atoms
$E$ activation energy, kcal/mol
$E_o$ intrinsic barrier, kcal/mol
$f$ smallest fraction of branched species mass breaking off
$F_n$ probability that a branched chain has $n$ branches
$\Delta H_r$ heat of reaction, kcal/mol
$i$ chain length in monomer units
$j$ chain length in monomer units
$k_{bbf}$ rate constant for the backbiting reaction forming a midchain radical, $s^{-1}$
$k_{bbr}$ rate constant for the backbiting reaction forming an end-chain radical, $s^{-1}$
$k_{bs}$ $\beta$-scission rate constant, $s^{-1}$
$k_c$ radical recombination rate constant, L/(mol s)
$k_d$ disproportionation rate constant, L/(mol s)
$k_{dp}$ depropagation rate constant (end-chain $\beta$-scission), $s^{-1}$
$k_f$ chain fission rate constant, $s^{-1}$
$k_{fb}$ rate constant for fission at a branch point, $s^{-1}$
$k_{fs}$ rate constant for fission at a specific location along a polymer chain, $s^{-1}$
$k_p$ propagation rate constant, L/(mol s)
$k_{ra}$ radical addition rate constant, L/(mol s)
$k_t$ termination rate constant, L/(mol s)
$k_t^o$ termination rate constant for chains of length 1, L/(mol s)
$k_{tr}$ chain transfer rate constant, L/(mol s)
$k_{tr}^o$ chain transfer rate constant for a radical of length 1, L/(mol s)
$k_{tr,e}$ chain transfer rate constant for the formation of a midchain radical from an end-chain radical, L/(mol s)
$k_{tr,m}$ chain transfer rate constant for the formation of an end-chain radical from a midchain radical, L/(mol s)
$m$ the $m$th moment of species
M symbol for monomer
$n$ chain length in monomer units
$N_{br}$ average number of branch points on branched species
$N_{ends}$ average number of chain ends on branched species
$p$ probability a branched chain has an additional branch
$p_A$ probability of type A branch point fission producing two branched species
$p_B$ probability of type B branch point fission producing a branched and a linear species
$p_C$ probability of type C nonbranch point fission producing two branched species
$p_D$ probability of type D nonbranch point fission producing a branched and a linear species
$r_s$ specific radical of length $s$
$s$ length of a specific radical in monomer units
$x$ chain length in monomer units
$y$ chain length in monomer units
$Re_i$ end-chain radical of length $i$
$Re^m$ $m$th moment of end-chain radicals, mol/L
$Rm_i$ midchain radical of length $i$
$Rm^m$ $m$th moment of midchain radicals, mol/L
$\alpha$ transfer coefficient
$\gamma$ diffusion dependence on chain length

## References and Notes


(1) Kruse, T. M.; Woo, O. S.; Broadbelt, L. J. *Chem. Eng. Sci.* **2001**, *56*, 971−979.
(2) Woo, O. S.; Broadbelt, L. J. *Catal. Today* **1998**, *40*, 121−140.
(3) Woo, O. S. Resource Recovery of Polystyrene to Monomer Through Binary Mixture Pyrolysis and Base Catalysis. Ph.D. Dissertation, Northwestern University, Evanston, IL, 1999.
(4) De Witt, M. J.; Dooling, D. J.; Broadbelt, L. J. *Ind. Eng. Chem. Res.* **1999**, *39*, 2228−2237.
(5) Menges, G.; Emminger, H.; Lackner, G. *Int. J. Mater. Prod. Technol.* **1991**, *6*, 307−330.
(6) Day, M.; Cooney, J. D.; Klein, C.; Fox, J. *Polym. Prepr. (Am. Chem. Soc., Div. Polym. Chem.)* **1993**, *34*, 123−124.
(7) Fouhy, K.; Kim, I.; Moore, S.; Culp, E. *Chem. Eng.* **1993**, *100* (12), 30−33.
(8) Shelly, S.; Fouhy, K.; Moore, S. *Chem. Eng.* **1992**, *99* (7), 30−35.
(9) Scott, D. S.; Majerski, P.; Piskorz, J.; Radlein, D.; Barnickel, M. *Can. J. Chem. Eng.* **1999**, *77* (7, October), 1021−1027.
(10) Aguado, J.; Serrano, D. *Feedstock Recycling of Plastic Wastes*; The Royal Society of Chemistry: Cambridge, U.K., 1999.
(11) Miller, A. *Environ. Sci. Technol.* **1994**, *28*, 16A.
(12) Wang, M.; Smith, J. M.; McCoy, B. J. *AIChE J.* **1995**, *41*, 1521−1533.
(13) Madras, G.; Smith, J. M.; McCoy, B. J. *Ind. Eng. Chem. Res.* **1996**, *35*, 1795−1800.
(14) Madras, G.; Chung, G. Y.; Smith, J. M.; McCoy, B. J. *Ind. Eng. Chem. Res.* **1997**, *36*, 2019−2024.
(15) Madras, G.; Smith, J. M.; McCoy, B. J. *Polym. Degrad. Stab.* **1997**, *58*, 131−138.
(16) Madras, G.; McCoy, B. J. *AIChE J.* **1998**, *44*, 647−655.
(17) Madras, G.; McCoy, B. J. *Ind. Eng. Chem. Res.* **1999**, *38*, 352−357.
(18) McCoy, B. J. *AIChE J.* **1993**, *39*, 1827−1833.
(19) McCoy, B. J.; Wang, M. *Chem. Eng. Sci.* **1994**, *49*, 3773−3785.
(20) McCoy, B. J.; Madras, G. *AIChE J.* **1997**, *43*, 802−810.
(21) Sezgi, N. A.; Cha, W. S.; Smith, J. M.; McCoy, B. J. *Ind. Eng. Chem. Res.* **1998**, *37*, 2582−2591.
(22) Teymour, F.; Campbell, J. D. *Macromolecules* **1994**, *27*, 2460−2469.
(23) Kodera, Y.; McCoy, B. J. *AIChE J.* **1997**, *43*, 3205−3214.
(24) Pladis, P.; Kiparissides, C. *Chem. Eng. Sci.* **1998**, *53*, 3315−3333.
(25) Wong, H.-W.; Broadbelt, L. J. *Ind. Eng. Chem. Res.* **2001**, *40*, 4716−4723.
(26) Faravelli, T.; Pinciroli, M.; Pisano, F.; Bozzano, G.; Dente, M.; Ranzi, E. *J. Anal. Appl. Pyrolysis* **2001**, *60*, 103−121.
(27) Daoust, D.; Bormann, S.; Legras, R.; Mercier, J. P. *Polym. Eng. Sci.* **1981**, *21* 721−726.
(28) Saidel, G. M.; Katz, S. *J. Polym. Sci., Part A-2* **1968**, *6*, 1149−1160.
(29) Odian, G. *Principles of Polymerization*; John Wiley & Sons: New York, NY, 1981; p 240.
(30) Giudici, R.; Hamielec, A. E. *Polym. React. Eng.* **1996**, *4*, 73−101.
(31) Evans, M. G.; Polanyi, M. *Trans. Faraday Soc.* **1938**, *34*, 11−29.
(32) Stein, S. E.; Lias, S. G.; Liebman, J. F.; Kafafi, S. A. *NIST Structures and Properties Users Guide*; National Institute of Standards and Technology, U.S. Department of Commerce: Washington, DC, 1994 (January).
(33) Tulig, T. J.; Tirrell, M. *Macromolecules* **1981**, *14*, 1501−1511.
(34) Cussler, E. L. *Diffusion: Mass Transfer in Fluid Systems*; Cambridge University Press: Cambridge, U.K., 1997; p 419.
(35) Rouse, P. E. J. *J. Chem. Phys.* **1953**, *21*, 1272−1280.
(36) O'Neil, G. A. An Examination of the Cause of the Gel Effect in Free Radical Polymerization. Ph.D. Dissertation, Northwestern University, Evanston, IL, 1998.
(37) de Gennes, P. G. *J. Chem. Phys.* **1982**, *76*, 3322−3326.
(38) Watanebe, M.; Tsukagoshi, M.; Hirakoso, H.; Adschiri, T.; Arai, K. *AIChE J.* **2000**, *46*, 843−856.
(39) Tobita, H.; Ito, K. *Polym. React. Eng.* **1993**, *1*, 407−425.
(40) Petzold, L. R. *DASSL Differential/Algebraic System Solver*; Sandia National Laboratories: Livermore, CA, 1983.
(41) Cameron, G. G.; Meyer, J. M.; McWalter, I. T. *Macromolecules* **1978**, *11*, 696−700.
(42) Willems, P. A.; Froment, G. F. *Ind. Eng. Chem. Res.* **1988**, *27*, 1959−1966.

(43) Griller, D. In *Radical Reaction Rates in Liquid*; Fischer, H., Ed.; Springer-Verlag: Berlin, 1984: Vol. 13a, p 12.
(44) Fried, J. R. *Polymer Science and Technology*; Prentice Hall Inc.: Upper Saddle River, NJ, 1995; p 33.
(45) Schreck, V. A.; Serelis, A. K.; Solomon, D. H. *Aust. J. Chem.* **1989**, *42*, 375−393.
(46) Deady, M.; Mau, A. W. H.; Moad, G.; Spurling, T. H. *Makromol. Chem.* **1993**, *194*, 1691−1705.
(47) Moad, G.; Solomon, D. H. *The Chemistry of Free Radical Polymerization*; Elsevier Science: Oxford, U.K., 1995; p 188.
(48) Gregg, R. A.; Mayo, F. R. *Discuss. Faraday Soc.* **1947**, *2*, 328−337.
(49) Kim, Y. S.; Hwang, G. C.; Bae, S. Y.; Yi, S. C.; Moon, S. K.; Kumazawa, H. *Kor. J. Chem. Eng.* **1999**, *16*, 161−165.
(50) Blowers, P.; Masel, R. I. *J. Phys. Chem. A* **1999**, *103*, 7047−7054.
(51) Hui, A. W.; Hamielec, A. E. *J. Appl. Polym. Sci.* **1972**, *16*, 749−769.
(52) Yang, M.; Shibasaki, Y. *J. Polym. Sci., Part A: Polym. Chem.* **1998**, *36*, 2315−2330.
(53) Bouster, C.; Vermande, F.; Veron, J. *J. Anal. Appl. Pyrolysis* **1980**, *1*, 297−313.

MA020490A